This is a repository copy of *Verification of an intelligent ray launching algorithm in indoor environments in the Ka-band*.

AGU
ADVANCING EARTH AND SPACE SCIENCE

Radio Science®

Key Points:
- Intelligent ray launching algorithm (IRLA) based channel simulations in three-dimensional (3-D) indoor environment models
- Radio channel measurements in indoor environments in the Ka-band of the millimeter-wave (mmWave) spectrum
- Comparison of power delay profiles (PDPs), path loss, and root-mean-square (RMS) delay spreads between simulation and measurement results

Correspondence to:
J. Zhang,
Jiliang.Zhang@sheffield.ac.uk

Verification of an Intelligent Ray Launching Algorithm in Indoor Environments in the Ka-Band

Wenfei Yang[1,2], Jie Huang[3,4], Jiliang Zhang[1] , Yuan Gao[2], Sana Salous[5] , and Jie Zhang[1,2]

[1]Department of Electronic and Electrical Engineering, The University of Sheffield, Sheffield, UK, [2]Ranplan Wireless Network Design Ltd, Cambridge, UK, [3]National Mobile Communications Research Laboratory, School of Information Science and Engineering, Southeast University, Nanjing, China, [4]Purple Mountain Laboratories, Nanjing, China, [5]Department of Engineering, Durham University, Durham, UK

Abstract This paper presents the verification of indoor propagation channel simulations based on an intelligent ray launching algorithm (IRLA) in the Ka-band of the millimeter-wave (mmWave) spectrum in various indoor environments, including a classroom, an office, and a corridor, by radio channel measurements. Power delay profiles (PDPs), path loss, and root-mean-square (RMS) delay spreads were obtained from both the simulation results and the measurement results. Moreover, parameters of two site-general path loss models, the close-in free space reference distance path loss model and the floating-intercept path loss model, were estimated based on the measured and simulated path loss. The comparison between the simulation results and the measurement results indicates that the IRLA-based simulation can accurately describe the main characteristics of the indoor propagation channel in the Ka-band.

1. Introduction

In wireless communication system design and network planning, ray-based deterministic approaches are widely employed to characterize the propagation channel (Hong et al., 2018; Yun & Iskander, 2015). They assume electromagnetic (EM) waves as rays that carry energy and follow the laws of propagation mechanisms, including line-of-sight (LoS), reflection, transmission, diffraction, and diffuse scattering. The trajectory of a transmitted EM wave is generated following geometrical optics (GO) rules. The ray-based deterministic approaches can be further classified into ray-tracing (RT) and ray-launching (RL) models. RT models predict the EM wave propagation given the locations of the transmitter (TX) and the receiver (RX). Whereas, RL models trace rays over the propagation environment without a specified RX location, which are more efficient for the multi-point radio frequency (RF) prediction in a wireless network (Fuschini et al., 2015).

As user demands increase rapidly, several millimeter-wave (mmWave) bands have been identified in the World Radiocommunications Conference in 2015 (WRC15) as candidate frequencies for 5G applications to enhance mobile radio capacity (Resolution 238, 2015). In WRC19, some of these mmWave bands have been agreed with 85% global harmonization, which includes 6.5 GHz in the frequency band from 37 to 43.5 GHz (Resolution 243, 2019). Nowadays, over 80% of data traffic takes place indoors (Cisco, n.d.). However, in complex indoor environments, EM waves in the mmWave bands are more vulnerable than those in conventional frequency bands due to the propagation characteristics (Rappaport et al., 2013; J. Zhang et al., 2018; H. Zhang et al., 2020). The ray-based deterministic approaches are considered promising for RF prediction in indoor mmWave wireless networks (Rappaport et al., 2014). The prediction accuracy can only be validated by practical channel measurements (Jacob et al., 2012; Pascual-García et al., 2015).

In this paper, we employ an intelligent ray launching algorithm (IRLA) to conduct RF prediction in three indoor environments, including a classroom, an office, and a corridor, at 37–41.5 GHz (Ka-band), and present the validation of the prediction accuracy by channel measurements (Yang et al., 2020). The IRLA was first proposed for fast and accurate RF prediction in urban scenarios in (Lai, Bessis, Roche, Song, et al., 2009). Then it was extended to indoor scenarios in (Lai et al., 2010, 2011). The IRLA-based simulations were validated by channel measurements for outdoor propagation prediction at 2.14 GHz in Lai et al. (2012), indoor propagation prediction at 3.5 and 60 GHz in (Lai et al., 2010, 2011; Weng et al., 2015), outdoor to indoor propagation prediction at 3.5 GHz in (Xia, Lai, Villemaud, & Zhang, 2015), and indoor to outdoor

propagation prediction at 2.4 GHz in (Xia, Lai, & Zhang, 2015). In the previous works, validation of IR-LA-based simulations was focused on the received signal strength. In this paper, the simulation results and the measurement results are compared in terms of the power delay profiles (PDPs), path loss, and root-mean-square (RMS) delay spreads on the measurement points in the three indoor environments. Moreover, two site-general path loss models, the close-in free space reference distance path loss model and the floating-intercept path loss model, are fitted from the simulated and measured path loss. The channel measurements were conducted using the multi-band custom-designed frequency modulated continuous wave (FMCW) channel sounder extended with new RF heads to cover the frequency band from 37 to 41.5 GHz (Salous et al., 2016).

The remainder of the paper is organized as follows. Section 2 describes the propagation environments and the configurations of the IRLA-based simulations. Section 3 describes the measurement equipment and setups. In Section 4, the numerical results obtained from simulations and measurements are compared and discussed. Finally, conclusions are drawn in Section 5.

2. IRLA-Based Channel Simulations

2.1. Propagation Environments

Figures 1 and 2 present the pictures and plans of the environments under measurement at Durham University, respectively. Descriptions of the propagation environments are as follows. (a) *Classroom*: as shown in Figure 1a, the classroom contains three rows of desks and other small objects, including chairs, a PC monitor, a projector, etc. It is 8.6 m in length, 7 m in width, and 2.8 m in ceiling height. There are three sizable exterior glass windows, which are 1.1 m above the floor, and a door, which is 1.5 m in width and 2 m in height. Outside the classroom is a long corridor connecting other rooms. (b) *Office*: as shown in Figures 1c and d, the office is 21 m in length, 7.4 m in width, and 2.8 m in ceiling height. There are storage cabinets, chairs, and desks with PC monitors. The office is divided into two separate spaces by a partition in the middle. (c) *Corridor*: as shown in Figure 1b, the corridor is 15.9 m in length, 1.9 m in width, and 2.8 m in ceiling height. A door is located at either end, which is 1.4 m in width and 2 m in height. There are laboratories and offices on either side of the corridor.

2.2. IRLA-Based Channel Simulations for Indoor Scenarios

To facilitate the mathematical computations, the IRLA discretizes the propagation environment into cube elements associated with a set of information, including the location and materials. The accuracy of the IRLA depends on the resolution of the environment discretization significantly. Using a high resolution may improve prediction accuracy but increases the time needed to conduct the simulation (Lu et al., 2019). Therefore, a tradeoff between the computational cost and the prediction accuracy is important for the IRLA. The IRLA was first presented in (Lai, Bessis, Roche, Song, et al., 2009) for urban scenarios, where the computations can be divided into three major components, (a) LoS, (b) vertical diffraction, and (c) horizontal diffraction and reflection, associated with the computations of LoS rays, rooftop diffraction rays, and horizontal diffraction and reflection rays, respectively. The angular dispersion for discrete RL models was addressed in (Lai, Bessis, Roche, Kuonen, et al., 2009) to complement the IRLA. To apply the IRLA in indoor scenarios, it was modified accordingly in (Lai et al., 2010, 2011). The programming implementation of the IRLA was demonstrated in (Lai, Bessis, Kuonen, et al., 2009) based on parallel object-oriented programming in C++. In this paper, the simulations were conducted in an IRLA-based RF planning tool (Ranplan Professional, n.d.).

To conduct the IRLA-based simulations, we first established the three-dimensional (3-D) environment models of the actual propagation environments, as shown in Figure 3. Main objects in the environments, including walls, floors, ceilings, cabinets, windows, doors, and desks, were expressed in the models, while other small objects, such as chairs and PC monitors, were omitted for simplification. The materials of the objects in the models were configured based on the measurement results in the actual environments. The computation resolution in the 3-D environment models was set to 0.1 m. The simulations were set for a maximum of five times of transmissions and five times of reflections. Diffraction was not counted for its effects are weak in the mmWave band (Maccartney et al., 2015).
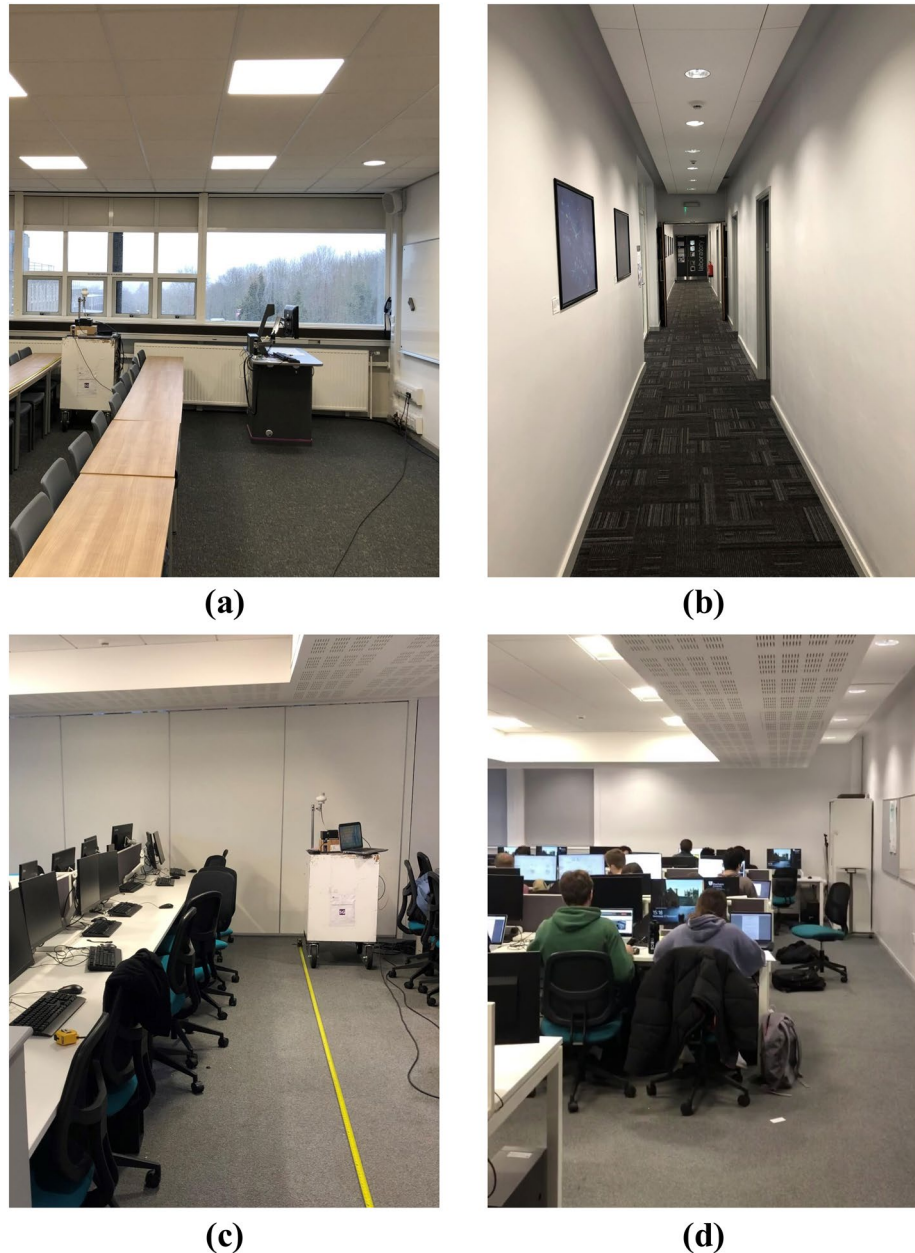
Figure 1. Propagation environments. (a) Classroom. (b) Corridor. (c) Office, line-of-sight (LoS). (d) Office, non-LoS (NLoS).

A network system operating in the frequency band of 37–41.5 GHz was used in the simulations. The RX antenna was set as an omnidirectional antenna of 1.6 m above the floor. The TX antenna was set as a directional antenna of 1.7 m above the floor. The radiation pattern of the directional antenna employed in the simulations and data analysis is shown in Figure 5, which was obtained by fitting a parabola to the practical radiation pattern. In the classroom and office environments, we conducted the simulations and channel measurements for both LoS and non-LoS (NLoS) scenarios. In the classroom environment shown in Figure 2a, the LoS TX antenna was located in a corner with the main lobe pointing to the direction 45° in azimuth, while the NLoS TX antenna was located in the corridor outside the room with the main lobe pointing to the direction 0° in azimuth. The simulations were conducted for LoS and NLoS scenarios separately. For the office environment shown in Figure 2b, the TX antenna was located near an interior wall with the main lobe pointing to the direction 0° in azimuth.
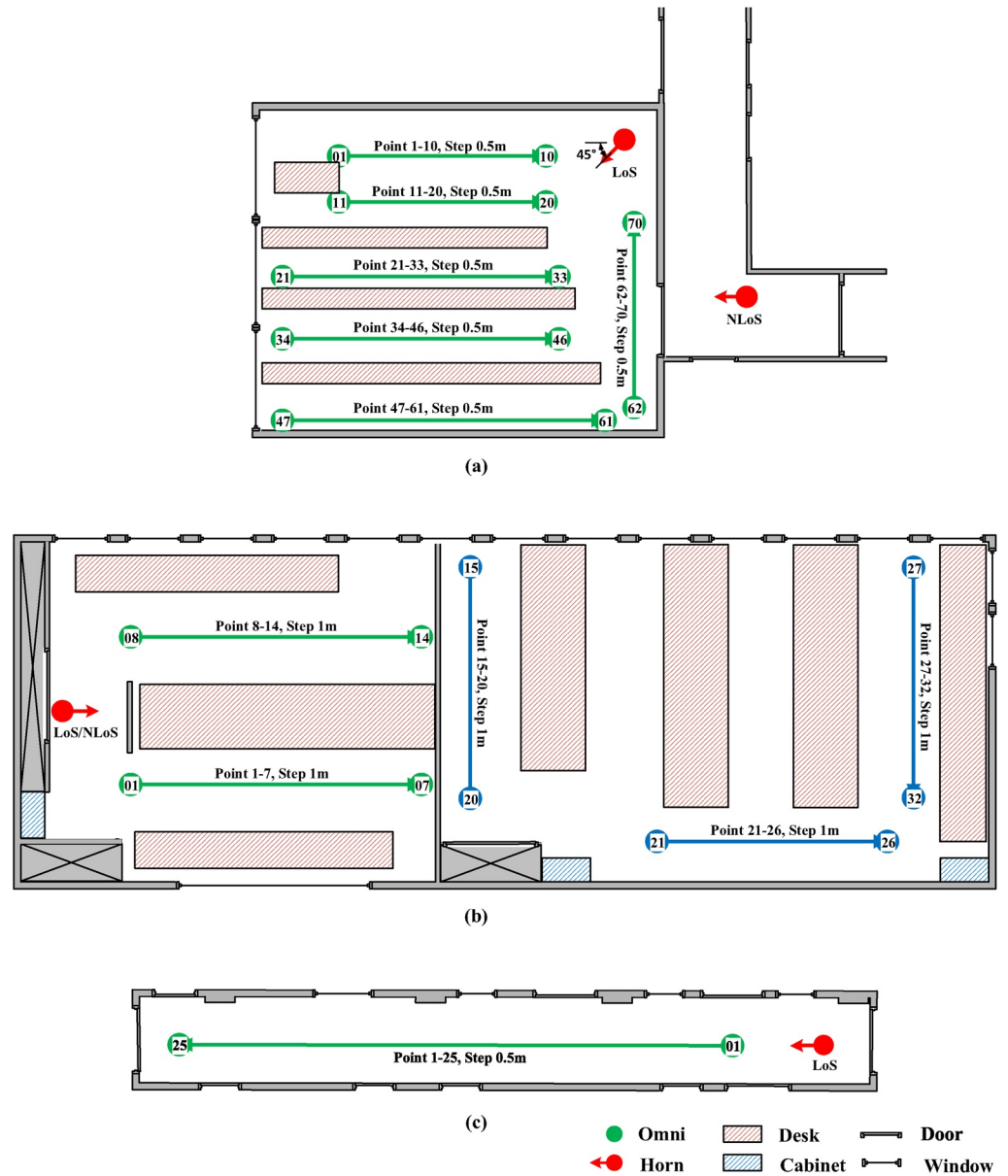
Figure 2. Plans of the propagation environments. (a) Classroom. (b) Office. (c) Corridor.

The LoS and NLoS measurement points were located on either side of the partition. For the corridor environment shown in Figure 2c, the TX antenna was located at an end of the corridor with the main lobe pointing to the direction 0° in azimuth. The port power of the TX antenna was set to 0 dBm in the three environments.

3. Measurement Equipment and Setups

3.1. Measurement Equipment

A custom-designed FMCW channel sounder at Durham University was used for the channel measurements (Salous et al., 2016). The sounder covers several frequency bands both below and above 6 GHz. With a programmable intermediate frequency from 12.5 to 18 GHz and frequency multipliers for the 25–30 GHz, 36–42 GHz, 50–75 GHz, and 60–90 GHz bands, channel measurements can be carried out with a maximum bandwidth of 3 GHz, 4.5 GHz, 6 GHz, and 9 GHz in the respective bands. Due to the high transmission
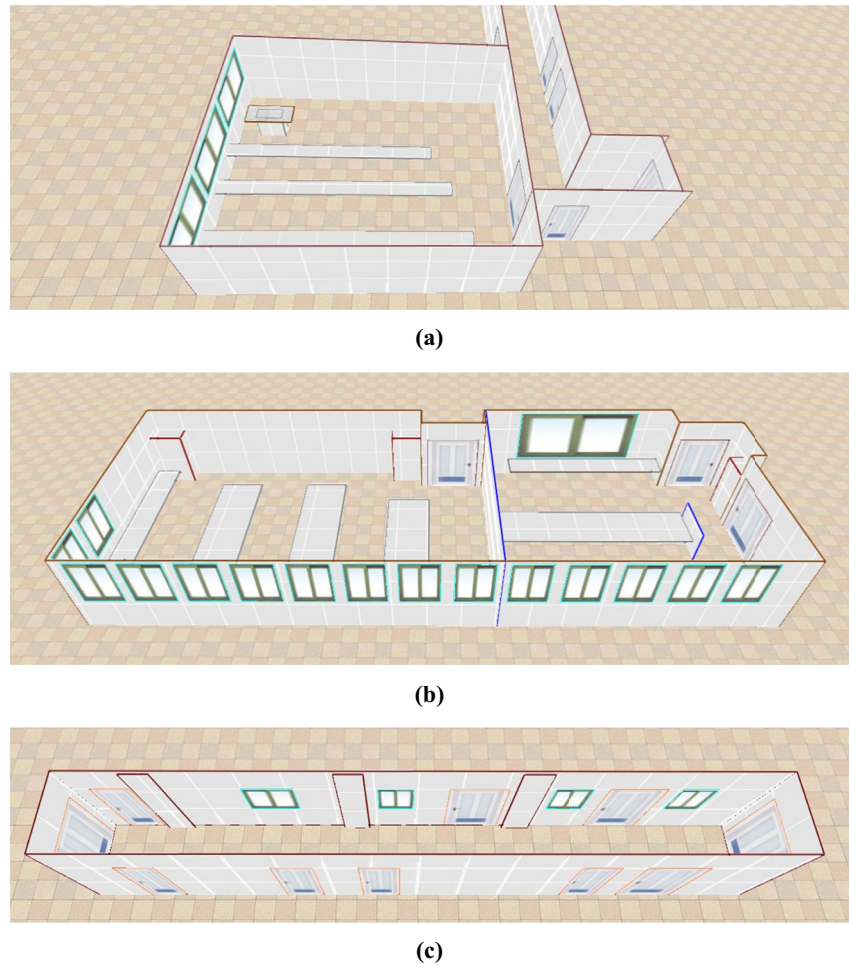
Figure 3. Simplified 3-D propagation environment models (Ranplan Professional, n.d.). (a) Classroom. (b) Office. (c) Corridor.

bandwidth, a heterodyne receiver architecture is used to compress the received signal and down-convert it to baseband, which can then be sampled at a low rate of 40 MHz. For the current measurements, the waveform repetition frequency used in the measurements was 1.22 kHz and the data were analyzed with a time delay resolution of 1 ns.

3.2. Measurement Setups

For channel measurements, assuming reciprocity, we fixed the RX unit on the TX locations marked by the red dots in Figure 2, while the TX unit was moved onto the measurement points indicated on the traces to imitate the users. The descriptions of the measurement points in each scenario are given in Table 1. An omnidirectional antenna of 1.6 m above the floor with a typical gain of ~5 dBi was selected as the TX antenna. A directional antenna of 1.7 m above the floor with a typical gain of ~ 10 dBi was employed as the RX antenna. The radiation pattern is shown in Figure 5. Both the TX and RX antennas were vertically polarized (V-V). Figure 4 presents the pictures of the TX unit and the RX unit. All doors in the environments shown in Figure 1 were kept closed during the measurements.

Table 1
Measurement Points in the Propagation Environments

Environment	LoS/NLoS	Measurement points	TX-RX separation [m]
Classroom	LoS	1–70	1.7–9.6
	NLoS	1–65	2.6–10.4
Office	LoS	1–14	2.1–7.5
	NLoS	15–32	8.8–18.9
Corridor	LoS	1–25	2.0–14.0

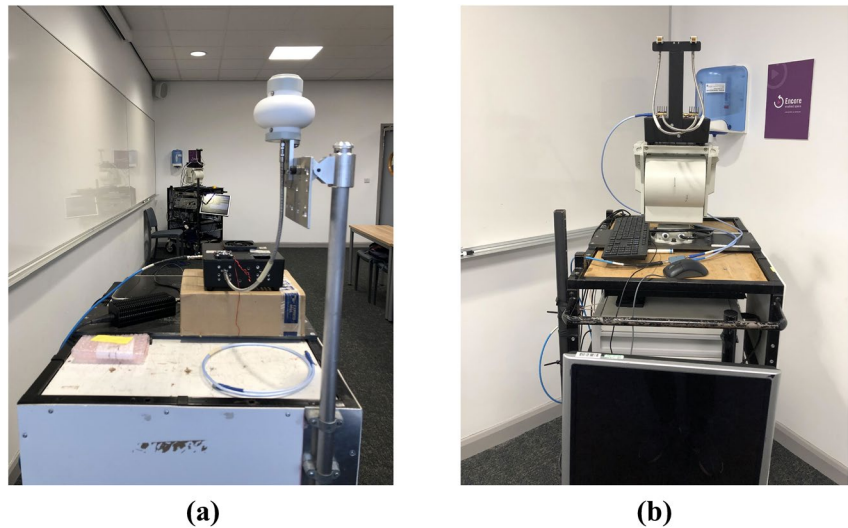*Note.* LoS, line-of-sight; NLoS, non-LoS; TX, transmitter; RX, receiver.

Figure 4. The mmWave channel sounder. (a) transmitter (TX). (b) receiver (RX).

4. Data Analysis and Results

4.1. Power Delay Profiles

The PDPs were estimated to compare the time delay and the power level of the multipath components (MPCs) between the simulation results and the measurement results. Figure 6 shows the PDPs for the measurement points in the three environments, where the simulated data were passed through a band-limited filter with a 1-GHz bandwidth to match the property of the channel sounder used in the measurements. For the MPCs with relatively high power, the simulation results show a good agreement with the measurement results in terms of both the relative time delay and the power level. For the MPCs with relatively low power, the simulations captured fewer MPCs than the measurements. The difference between the simulation results and the measurement results could be attributed to the following. (a) Configurations of the propagation mechanisms in the IRLA-based simulations. The simulations counted a maximum of five times of reflections and did not consider the effects of diffraction and scattering. However, the channel sounder could detect scattered, diffracted, and multiply reflected MPCs, which were not included in the simulation results. (b) Configurations of the devices and materials. The approximation to the radiation pattern of the antenna might induce error to the simulation results. The difference exists between the loss caused by practical construction materials and the materials defined in the 3-D environment models. (c) Simplified 3-D environment models. The 3-D environment models were simplified from the practical environments, which omitted the small objects, such as chairs and PC monitors. Moreover, the models were established for the target rooms, where the environments outside the target rooms were not considered. Consequently, the MPCs which resulted from the omitted small objects or structures of other rooms could not be related to the simulation results.
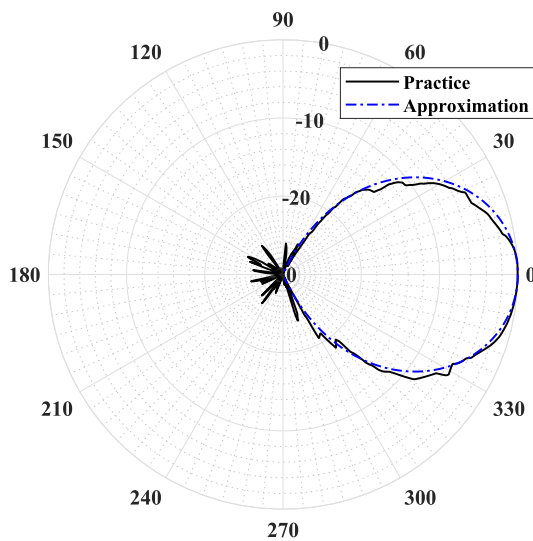
4.2. Site-General Path Loss Models

Path loss refers to the ratio of the transmitted power and the received power, excluding the overall system gain and antenna gains. Site-general path loss models with mathematically tractable formats provide practical insights into propagation channel characterization. Conventionally, site-general path loss models are fitted from measured data in typical propagation environments and assumed to be generally valid in similar scenarios (Maccartney et al., 2015; Salous & Gao, 2016; J. Zhang
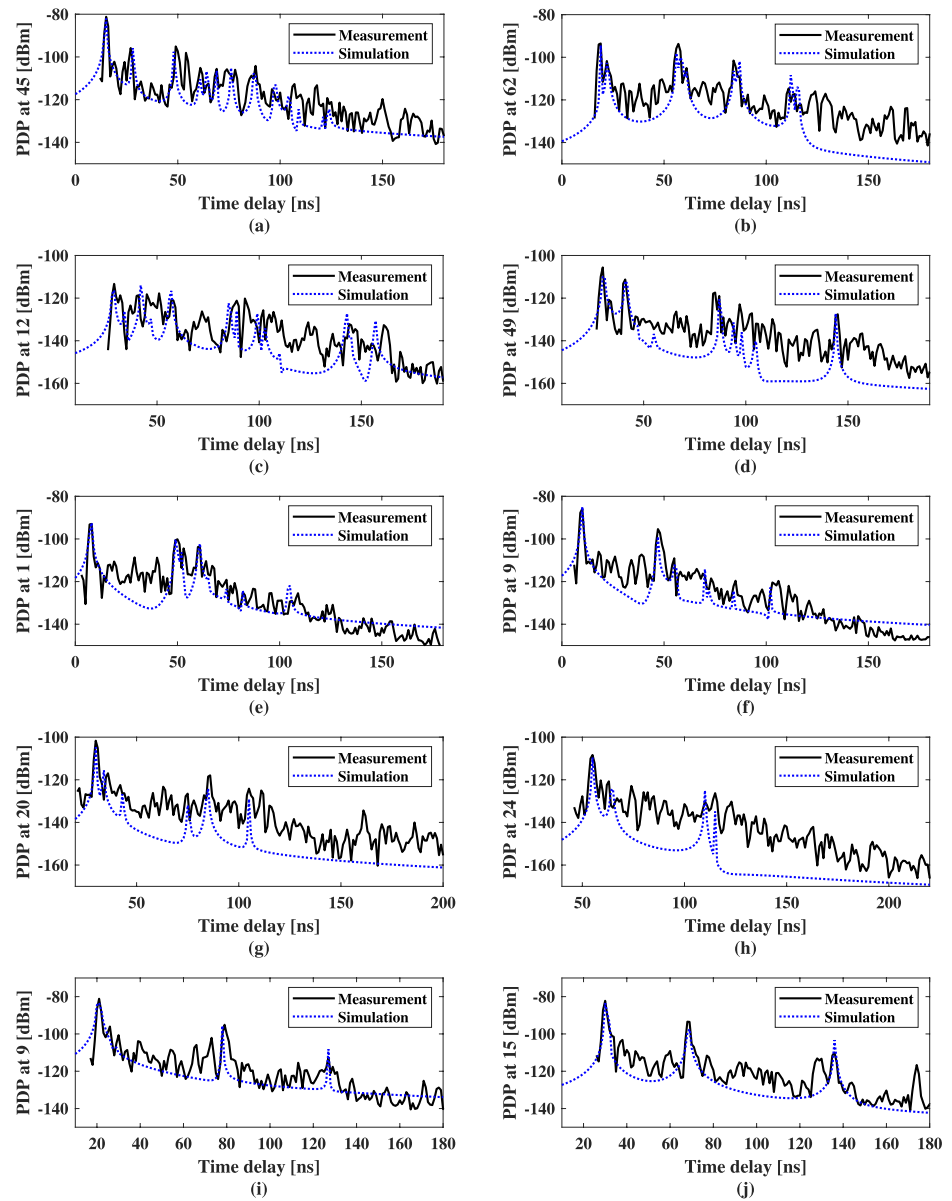

Figure 5. The radiation pattern of the directional antenna on the H-plane in dB.

Figure 6. Comparison of power delay profiles (PDPs). (a and b) classroom, line-of-sight (LoS). (c and d) classroom, non-LoS (NLoS). (e and f) office, LoS. (g and h) office, NLoS. (i and j) corridor.

et al., 2014). Consequently, the measurement-based site-general models may induce considerable error when a target environment and the measured environment differ significantly. The IRLA-based simulation can be considered as an alternative way to obtain site-general path loss models, for it captures the path loss of the TX-RX links in a specific environment. Here we generate and compare two typical site-general models, the close-in free space reference distance path loss model and the floating-intercept path loss model, from measured and simulated path loss for the LoS scenarios. The obtained models could also be extended to similar indoor scenarios. The close-in free space reference distance path loss model and the floating-intercept path loss model are referred to as the CI model and the FI model in the following, respectively.

The CI model has been widely used in studies of mmWave propagation (Maccartney et al., 2015) and adopted in the ITU standards for indoor environments (Recommendation ITU-R P.1238-10, 2019). The free space path loss at a reference close-in distance is taken as a physically based anchor. The CI model is given by

Table 2
Site-General Path Loss Models. q_{PL} Denotes the RMSE Between Simulated and Measured Data

| Environment | q_{PL} [dB] | Data | CI model | | FI model | | |
			n	σ_{CI} [dB]	β	α	σ_{FI} [dB]
Classroom	2.71	Measurement	1.52	2.00	1.99	60.78	1.80
		Simulation	1.80	1.27	1.62	65.60	1.23
Office	1.03	Measurement	1.93	1.47	2.52	60.24	0.97
		Simulation	1.96	0.96	2.29	62.07	0.74
Corridor	1.72	Measurement	1.80	1.52	1.58	66.29	1.42
		Simulation	1.88	0.44	1.84	64.69	0.43

Note. RMSE, root-mean-square error.

$$PL(f,d)[dB] = FSPL\left(f,d_0\right) + 10 \cdot n \log_{10}\left(\frac{d}{d_0}\right) + X_\sigma^{CI}, \qquad (1)$$

where n is the path loss exponent (PLE), d is the 3-D TX-RX separation in meters, and X_σ^{CI} is a zero mean Gaussian random variable with the standard deviation σ_{CI} in dB. The physically based anchor is computed by

$$FSPL\left(f,d_0\right)[dB] = 20 \log_{10}\left(\frac{4\pi d_0 f}{c}\right), \qquad (2)$$

where d_0 is the reference close-in distance, $c = 3 \times 10^8$ ms^{-1} is the speed of light, and f is the carrier frequency in Hz. Using $d_0 = 1$ m, we have $FSPL\left(f,d_0\right) = 64.32$ dB at 39.25 GHz. In the ITU standards (Recommendation ITU-R P.1238-10, 2019, Table 2), a CI model is reported for a typical LoS office scenario in the 38-GHz band, where the PLE $n = 2.03$ and the standard deviation $\sigma_{CI} = 4.6$ dB. Another commonly used site-general model is the FI model, which has been adopted in the WINNER II and 3GPP standards (3GPP TR 38.901 V14.1.1, 2017; Kyösti et al., 2008). It requires two parameters and does not consider a physically based anchor, as

$$PL(d)[dB] = \alpha + 10 \cdot \beta \log_{10}(d) + X_\sigma^{FI}, \qquad (3)$$

where α is the floating-intercept in dB, β is the slope, and X_σ^{FI} is a zero mean Gaussian random variable with the standard deviation σ_{FI} in dB.
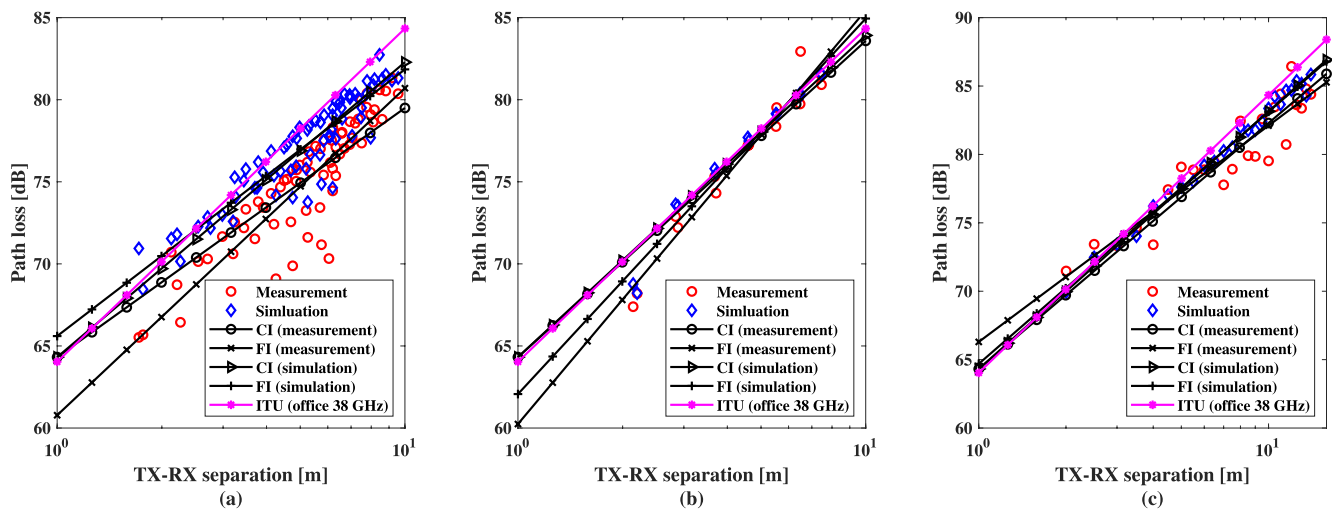

Figure 7. Measured and simulated path loss, the fitted site-general models, and the 38-GHz ITU office model. (a) Classroom, line-of-sight (LoS). (b) Office, LoS. (c) Corridor.
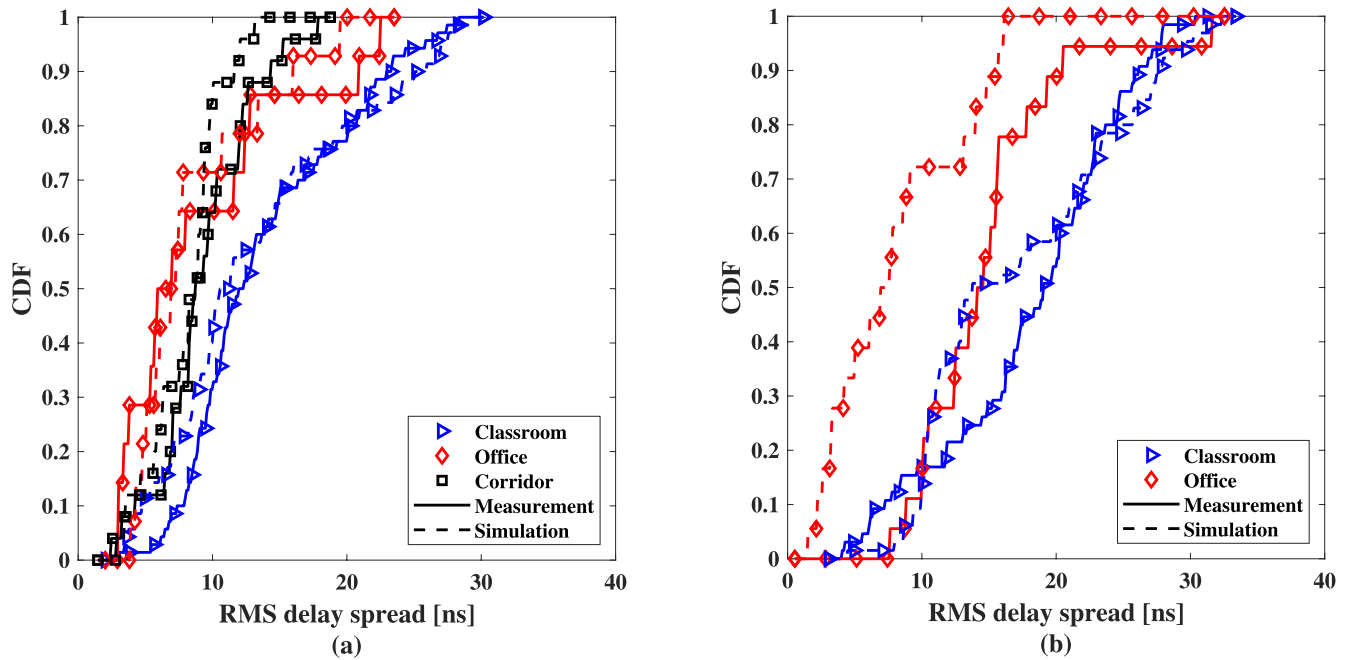
Figure 8. The cumulative distribution functions (CDFs) of the root-mean-square (RMS) delay spreads. (a) line-of-sight (LoS) scenarios. (b) non-LoS (NLoS) scenarios.

The CI model and the FI model were obtained from the measured and simulated path loss by minimum mean square error (MMSE) fitting. A noise exclusion threshold of 30 dB was considered in the generation of the numerical results for both simulations and measurements. Figure 7 presents the measured and simulated path loss, the fitted site-general models, and the 38-GHz ITU office model. Table 2 gives the values of the parameters in the CI and FI models and the root-mean-square error (RMSE) between the measured and simulated path loss. Path loss obtained from the simulations and the measurements show similar trends but different values. The simulation-based models show smaller standard deviations of the shadow fading, that is, σ_{CI} and σ_{FI}, due to the simplified environment models. As the measurements were primarily LoS, the estimated intercept of the FI model from the simulated data varies between 62.07 and 65.60 dB, which is close to the close-in free space reference value of 64.32 dB. The PLEs of the CI models obtained from both the simulations and the measurements are less than 2, that is the theoretical free space PLE, indicating that

Table 3
Comparison of Mean, Standard Deviation, Minimum and Maximum Values of the RMS Delay Spreads in ns. q_{DS} Denotes the RMSE Between Simulated and Measured Data

Environment	LoS/NLoS	q_{DS}	Data	$E[\sigma_\tau]$	σ	Min.	Max.
Classroom	LoS	3.11	Measurement	13.94	6.02	3.07	28.33
			Simulation	13.29	7.16	3.22	29.24
	NLoS	8.49	Measurement	18.13	6.66	4.08	30.40
			Simulation	17.24	7.29	4.49	32.39
Office	LoS	3.34	Measurement	8.98	6.12	3.02	22.55
			Simulation	8.52	4.55	3.95	19.52
	NLoS	10.05	Measurement	14.78	5.32	7.67	31.62
			Simulation	7.91	4.80	1.54	16.17
Corridor	LoS	3.24	Measurement	9.33	3.52	2.47	17.84
			Simulation	8.06	2.62	2.82	13.18

Note. LoS, line-of-sight; NLoS, non-LoS; RMS, root-mean-square; RMSE, root-mean-square error.

the propagation channel experienced constructive interference from bounce reflections in the measured environments. Compared with the ITU office model, the simulation-based CI model shows closer PLEs and standard deviations to the corresponding measurement-based models. In wireless network design, the simulation-based site-general models can be employed to characterize the propagation channel in a given indoor environment.

4.3. Root-Mean-Square Delay Spreads

The time dispersion properties of a wideband channel are characterized by the RMS delay spread, which is one of the fundamental parameters considered in wireless system design (Maccartney et al., 2015; Sun et al., 2014). The RMS delay spread is the square root of the second central moment of the PDP, as

$$\sigma_\tau = \sqrt{\frac{\sum_k P(\tau_k)\tau_k^2}{\sum_k P(\tau_k)} - (\overline{\tau})^2}, \tag{4}$$

where τ_k is the relative time delay for the k-th component arriving at the RX and $P(\tau_k)$ is the power of the k-th component. The mean excess delay $\overline{\tau}$ is computed by

$$\overline{\tau} = \frac{\sum_k P(\tau_k)\tau_k}{\sum_k P(\tau_k)}. \tag{5}$$

Figures 8a and 8b show the cumulative distribution functions (CDFs) of the RMS delay spreads for the 30 dB threshold below the peak over the LoS and the NLoS measurement points, respectively. Table 3 compares the mean, standard deviation, minimum, and maximum values of the RMS delay spreads obtained from the simulation results and the measurement results. For the LoS scenarios, the differences of the mean RMS delay spreads are less than 2 ns and the RMSE is less than 4 ns. As shown in Figure 8b, the RMS delay spreads obtained from the simulated data are smaller than those generated based on the measurements for the NLoS scenario of the office environment. It could result from the significant simplification to the environment model, where multiple objects enriching the MPCs were omitted. In general, the results indicate that the IRLA-based simulation can be used to describe the time dispersion properties in a realistic environment.

5. Conclusions

This paper presents a measurement-based validation of the IRLA in three indoor environments in the Ka-band of the mmWave spectrum. The results generated by the IRLA-based simulations were compared with the results of channel measurements in terms of the PDPs, path loss, and RMS delay spreads. The results have shown that the IRLA-based simulation can be considered as a reliable solution to predict the mmWave propagation channel in indoor scenarios for wireless communication system design and network planning. In future works, the prediction accuracy of the IRLA-based simulation will be investigated in other environments and frequency bands.

Data Availability Statement

The data are deposited in a publicly accessible domain and can be found in the link below: https://doi.org/10.6084/m9.figshare.14842380.

References

3GPP TR 38.901 V14.1.1. (2017). *Studay on channel model for frequencies from 0.5 to 100 GHz.* (Release 14).

Cisco. (n.d.). Cisco vision: 5G-thriving indoors. White Paper. Retrieved from. https://www.cisco.com/c/dam/en/us/solutions/collateral/service-provider/ultra-services-platform/5g-ran-indoor.pdf

Fuschini, F., Vitucci, E. M., Barbiroli, M., Falciasecca, G., & Degli-Esposti, V. (2015). Ray tracing propagation modeling for future small-cell and indoor applications: A review of current techniques. *Radio Science*, *50*(6), 469–485. https://doi.org/10.1002/2015rs005659

Hong, Q., Zhang, J., Zheng, H., Li, H., Hu, H., Zhang, B., et al. (2018). The impact of antenna height on 3D channel: A ray launching based analysis. *Electronics*, *7*(2), 1–13. https://doi.org/10.3390/electronics7010002

Jacob, M., Priebe, S., Dickhoff, R., Kleine-Ostmann, T., Schrader, T., & Kurner, T. (2012). Diffraction in mm and sub-mm wave indoor propagation channels. *IEEE Transactions on Microwave Theory and Techniques*, *60*(3), 833–844. https://doi.org/10.1109/tmtt.2011.2178859

Kyösti, P., Meinila, J., Hentila, L., Zhao, X., Jamsa, T., Schrader, T., et al. (2008). *WINNER II channel models*. IST-4-027756 WINNER II D1.1.2 V1.2.

Lai, Z., Bessis, N., Kuonen, P., Roche, G., Zhang, J., & Clapworthy, G. (2009). A performance evaluation of a grid-enabled object-oriented parallel outdoor ray launching for wireless network coverage prediction. In: *5th International Conference on Wireless and Mobile Communications* (pp. 38–43). https://doi.org/10.1109/icwmc.2009.14

Lai, Z., Bessis, N., Roche, G., Kuonen, P., Zhang, J., & Clapworthy, G. (2009). A new approach to solve angular dispersion of discrete ray launching for urban scenarios. In: *Loughborough Antennas Propagation Conference* (pp. 133–136). https://doi.org/10.1109/lapc.2009.5352420

Lai, Z., Bessis, N., Roche, G., Kuonen, P., Zhang, J., & Clapworthy, G. (2010). On the use of an intelligent ray launching for indoor scenarios. In: *4th European Conference on Antennas and Propagation* (pp. 1–5).

Lai, Z., Bessis, N., Roche, G., Song, H., Zhang, J., & Clapworthy, G. (2009). An intelligent ray launching for urban prediction. In: *3rd European Conference on Antennas and Propagation (EuCAP)* (pp. 2867–2871).

Lai, Z., Roche, G., Bessis, N., Kuonen, P., Clapworthy, G., Zhou, D., & Zhang, J. (2011). Intelligent ray launching algorithm for indoor scenarios. *Radio Engineering*, *20*(2).

Lai, Z., Song, H., Wang, P., Mu, H., Wu, L., & Zhang, J. (2012). Implementation and validation of a 2.5D intelligent ray launching algorithm for large urban scenarios. In: *6th European Conference on Antennas and Propagation (EuCAP)* (pp. 2396–2400). https://doi.org/10.1109/eucap.2012.6205808

Lu, J. S., Vitucci, E. M., Degli-Esposti, V., Fuschini, F., Barbiroli, M., Blaha, J. A., & Bertoni, H. L. (2019). A discrete environment-driven GPU-based ray launching algorithm. *IEEE Transactions on Antennas and Propagation*, *67*(2), 1180–1192. https://doi.org/10.1109/tap.2018.2880036

Maccartney, G. R., Rappaport, T. S., Sun, S., & Deng, S. (2015). Indoor office wideband millimeter-wave propagation measurements and channel models at 28 and 73 GHz for ultra-dense 5G wireless networks. *IEEE Access*, *3*, 2388–2424. https://doi.org/10.1109/access.2015.2486778

Pascual-García, J., Martínez-Inglés, M., Molina-García-Pardo, J., Rodríguez, J., & Llácer, L. J. (2015). Using tuned diffuse scattering parameters in ray tracing channel modeling. In: *9th European Conference on Antennas and Propagation (EuCAP)* (pp. 1–4).

Ranplan Professional. (n.d.). Retrieved from https://ranplanwireless.com/products/ranplan-professional/

Rappaport, T. S., Heath, R. W., Jr., Daniels, R. C., & Murdock, J. N. (2014). *Millimeter wave wireless communications*. Prentice-Hall.

Rappaport, T. S., Sun, S., Mayzus, R., Zhao, H., Azar, Y., Wang, K., et al. (2013). Millimeter wave mobile communications for 5G cellular: It will work! *IEEE Access*, *1*, 335–349. https://doi.org/10.1109/access.2013.2260813

Recommendation, ITU-R P. 1238-10. (2019). *Propagation data and prediction methods for the planning of indoor radiocommunication systems and radio local area networks in the frequency range 300 MHz to 450 GHz*.

Resolution 238. (2015). Studies on frequency-related matters for international mobile telecommunications identification including possible additional allocations to the mobile services on a primary basis in portion(s) of the frequency range between 24.25 and 86 GHz for the future development of international mobile telecommunications for 2020 and beyond. In *Proceedings of the world radio communications conference (WRC)*.

Resolution 243. (2019). Terrestrial component of international mobile telecommunications in the frequency bands 37-43.5 GHz and 47.2-48.2 GHz. In *Proceedings of the world radio communications conference (WRC)*. Sharm el-Sheikh.

Salous, S., Feeney, S. M., Raimundo, X., & Cheema, A. A. (2016). Wideband MIMO channel sounder for radio measurements in the 60 GHz band. *IEEE Transactions on Wireless Communications*, *15*(4), 2825–2832. https://doi.org/10.1109/twc.2015.2511006

Salous, S., & Gao, Y. (2016). Wideband measurements in indoor and outdoor environments in the 30 GHz and 60 GHz bands. In: *10th European Conference on Antennas and Propagation (EuCAP)* (pp. 1–3). https://doi.org/10.1109/eucap.2016.7481454

Sun, S., Rappaport, T. S., Heath, R. W., Nix, A., & Rangan, S. (2014). MIMO for millimeter-wave wireless communications: Beamforming, spatial multiplexing, or both? *IEEE Communications Magazine*, *52*(12), 110–121. https://doi.org/10.1109/mcom.2014.6979962

Weng, J., Tu, X., Lai, Z., Salous, S., & Zhang, J. (2015). Modelling the mmwave channel based on intelligent ray launching model. In: *9th European Conference on Antennas and Propagation (EuCAP)* (pp. 1–4).

Xia, B., Lai, Z., Villemaud, G., & Zhang, J. (2015). Joint ray launching method for outdoor to indoor propagation prediction based on interpolation. In: *9th European Conference on Antennas and Propagation (EuCAP)* (pp. 1–5).

Xia, B., Lai, Z., & Zhang, J. (2015). Joint ray launching method for indoor to outdoor propagation prediction based on ray aggregation. In: *9th European Conference on Antennas and Propagation (EuCAP)* (pp. 1–5).

Yang, W., Huang, J., Zhang, J., Salous, S., & Zhang, J. (2020). Indoor measurement based verification of ray launching algorithm at the Ka-band. In: *XXXIII General Assembly and Scientific Symposium of the International Union of Radio Science* (pp. 1–4). https://doi.org/10.23919/ursigass49373.2020.9232150

Yun, Z., & Iskander, M. F. (2015). Ray tracing for radio propagation modeling: Principles and applications. *IEEE Access*, *3*, 1089–1100. https://doi.org/10.1109/access.2015.2453991

Zhang, H., Shao, Y., Liao, X., Zhang, J., & Zhang, J. (2020). Measurement based millimeter wave massive MIMO channel parameter comparison. In: *14th European Conference on Antennas and Propagation (EuCAP)* (pp. 1–5). https://doi.org/10.23919/eucap48036.2020.9135293

Zhang, J., Glazunov, A. A., Yang, J., Chu, X., & Zhang, J. (2018). An experimental study on indoor massive 3D-MIMO channel at 30-40 GHz band. In: *International Symposium on Antennas and Propagation (ISAP)* (pp. 1–2).

Zhang, J., Yang, W., Ding, L., Huang, X., & Zhang, N. (2014). MIMO channel measurement and characterization at 6.0-6.4 GHz under typical classroom environment. *Journal of Harbin Institute of Technology*, *21*(1), 69–76.